Comparison Study of Morphology and Crystallization Behavior of Polyethylene and Poly(ethylene oxide) on Single-Walled Carbon Nanotubes

ARTICLE *in* THE JOURNAL OF PHYSICAL CHEMISTRY B · JULY 2010

Impact Factor: 3.3 · DOI: 10.1021/jp103932b · Source: PubMed

2 AUTHORS, INCLUDING:

Xiaoli Zheng
The Hong Kong University of Science and T…

26 PUBLICATIONS **292** CITATIONS

SEE PROFILE

Comparison Study of Morphology and Crystallization Behavior of Polyethylene and Poly(ethylene oxide) on Single-Walled Carbon Nanotubes

Xiaoli Zheng and Qun Xu*

College of Materials Science and Engineering, Zhengzhou University, Zhengzhou 450052, China

Received: April 30, 2010; Revised Manuscript Received: May 26, 2010

In this work, we provided a comparison study of morphology and crystallization behavior of polyethylene (PE) and poly(ethylene oxide) (PEO) on single-walled carbon nanotubes (SWNTs) with assistance of supercritical CO_2. The resulting polymer/SWNT nanohybrids were characterized by transmission electron microscopy, scanning electron microscopy, Fourier transform infrared spectroscopy, Raman spectra, wide-angle X-ray diffraction, and differential scanning calorimetry. SWNT small bundles were decorated by PE lamellar crystals, forming nanohybrid "shish-kebab" (NHSK) structure, whereas SWNTs were only wrapped by a thin amorphous polymer coating in the case of PEO. The varying morphologies of the nanohybrids were found to depend on the molecular conformation and the interactions between polymer chains and SWNTs. Nonisothermal experiments showed that SWNTs provided heterogeneous nucleation sites for PE crystallization, while the NHSK structure hindered polymer chain diffusion and crystal growth. Also, SWNTs played antinucleation effect on PEO. In addition, the formation mechanism analysis indicated that PE chains preferred to form a homogeneous coating along the tube axis before proceeding to kebab crystal growth. The purpose of this work is to enlarge the area of theoretical understanding of introducing precisely hierarchical structures on carbon nanotubes, which are important for functional design in nanodevice applications.

Introduction

During the past decade, modification of carbon nanotubes (CNTs) has been of great interest due to the lack of solubility and the difficult manipulation in any solvents of CNTs.[1,2] The main approaches for modification of these quasi one-dimensional structures can be grouped into two categories: chemical functionalization techniques and noncovalent wrapping methods.[3−8] The noncovalent functionalization of CNTs is particularly attractive because it offers the possibility of attaching chemical handles without affecting the electronic network of the tubes based on van der Waals forces or $\pi-\pi$ stacking.[5−8] Macromolecules such as polymers and biomolecules noncovalent wrapping CNTs have been widely studied for their potential applications, including polymer composites and biosensors.[9−12]

Studies on the interrelation between the interfacial interaction of polymer with CNTs and the morphology of polymer on the CNT surfaces have received considerable attention.[13,14] Many researchers have studied the intermolecular interaction energy between polymer molecules and CNTs by performing molecular dynamics (MD) simulations.[15−17] They showed that the intermolecular interaction is strongly influenced by the specific monomer structure of polymer, and polymers with backbones containing aromatic rings are promising candidates for the noncovalent binding of CNTs into composite structures. Both Yang et al. and Liu et al. proposed that the polyethylene (PE) chains preferred the extended conformation or ordered orientation structure along the CNTs axis by the attractive van der Waals interactions in the first adsorption layer.[18,19] Interactions between polymer molecules and carbon nanotubes and thus the molecule structures are crucial for effective load transfer from polymer matrix to CNTs.[20,21] Cadek et al.[22] reported that Young's modulus of poly(vinyl alcohol) (PVA) could be increased when the crystalline polymer coating formed at the multiwalled carbon nanotubes (MWNTs) surface. However, using similar MWNTs and noncrystalline polymer resulted in much lower levels of reinforcement. It seems right that well-ordered polymers on the CNT surface are vital for effective stress transfer. Zhang et al. reported that a number of molecular structural variables, including chain regularity, thermodynamic chain flexibility in solution, and orientation of crystal growth induced by CNTs can affect the polymer supermolecular structures on CNTs.[23] Ning et al. investigated the effect of molecular weight of the PE matrix on the formation of polyethylene/inorganic whisker hybrid shish kebab structure and indicated that the nucleation efficiency of inorganic whisker was decreased with increasing molecular weight of PE.[24]

The structure of the nucleated crystalline polymer layer on CNTs is of particular interest. In recent years, crystalline polymer/CNT nanocomposites are one of the most promising fields for CNTs that not only can provide nucleation sites but also can accelerate the growth of polymer crystals, which have distinct advantages for efficiently improving mechanical properties of the nanocomposites.[25−28] Periodic patterning of CNTs with crystalline polymers, especially the novel nanohybrid shish-kebab (NHSK) superstructure in which fibrillous CNTs act as shish while polymer lamellae as kebab has attracted more attentions.[29−37] In our study, linear high density PE was periodically decorated on single-walled carbon nanotubes (SWNTs) and MWNTs by a supercritical CO_2 antisolvent-induced polymer epitaxy (SAIPE) method.[34,35] In comparison to the traditional solution crystallization method,[29,37] as an antisolvent to induce polymer crystallization or epitaxy, SC CO_2 is more benign to the environment and is easily controllable in experimental conditions. This hierarchical nanostructure is more robust compared with the surfactant and small molecular wrapping since it is the rigid single crystals on the CNTs that are expected to be used in the field of nanocomposites to catalyst

* To whom correspondence should be addressed. E-mail: qunxu@zzu.edu.cn. Tel.: +86 371 67767827. Fax: +86 371 67767827.

10.1021/jp103932b
Published on Web 07/02/2010

supports.[38] Fabrication and characterization of hierarchical carbon nanostructures have been intensively studied for their potential applications.[39−41] However, in the case of poly(ethylene oxide)/CNT nanocomposites, it has been reported that CNTs did not act as a nucleation agent for PEO and the crystal growth of PEO were severely restricted by the incorporation of CNTs.[42,43] Li et al. also indicated that PEO did not crystallize on pristine CNTs because of the unfavorable interaction between CNTs and the PEO chains.[44] In our previous study, periodic-patterning nanocrystals of water-soluble polymers such as poly(vinyl alcohol) (PVA) and poly(ethylene glycol) (PEG) wrapping on the SWNTs were successfully achieved in supercritical CO_2 (SC CO_2) antisolvent process, and the PVA/CNT NHSK structure was also obtained.[36] Some groups have also found that CNTs can act as nucleation agents for PVA.[45,46] As we all know, both PEO and PVA are water-soluble crystalline polymers, whereas the different results that appeared in the polymer/CNT composites is interesting.

In this paper, we choose two kinds of representative polymers, high molecular weight linear PE and water-soluble, biocompatible PEO, to study their morphology and crystallization behavior on the surface of SWNTs with assistance of SC CO_2.

Experimental Section

Materials. The SWNTs were supplied by Carbon Nano Materials R&D Center, Chengdu Desran Technology Co., Ltd. (China) with a purity of 80 wt %. The MWNTs were purchased from Aldrich. They were purified with mixed acid (sulfuric acid and nitric acid at the ratio of 3:1 by volume) before used.[35] Linear polyethylene (PE, melt flow index MFI = 12 g/10 min) and poly(ethylene oxide) (PEO, number-average molecular weight M_n = 300K g/mol) were purchased from Aldrich. *p*-Xylene, 1,2-diclorobenzene (DCB), and *N*,*N*-dimethylformamide (DMF) were all purchased from Sinopharm Chemical Reagent Co., Ltd. (China) and used as received.

Samples Preparation. PE/SWNT nanohybrid was obtained by the SC CO_2 SAIPE method.[35] Both *p*-xylene and DCB were used as the solvent for PE. For PEO, the similar procedure was adopted and DMF was used as the solvent. A 0.5 mg sample of PEO was dissolved in 4 g of DMF at a suitable temperature. A 0.1 mg sample of SWNTs was dispersed in 1 g of DMF and ultrasonicated for 1 h before being added into PEO/DMF solution. The mixture was then quickly transferred into the SC CO_2 apparatus to reach the determined conditions of temperature and pressure. The reaction time in the condition of SC CO_2 was controlled to be 3 h and then the system was slowly depressurized and the sample was collected. Comparison studies were also made by treating the pure polymer in the same SC CO_2 condition as the corresponding nanohybrid prepared.

Characterization. Transmission electron microscopy (TEM) (FEI Tecnai G2 20) experiments were conducted with an accelerating voltage of 120 kV. A field-emission scanning electron microscope (SEM) (JEOL JSM-6700F) was used to characterize the morphology of the polymer functionalized CNTs. FT-IR spectra were recorded using a BRUKE TENSOR27 instrument with a resolution of 2 cm^{-1}. KBr was used to prepare sample pellets. Raman spectra were obtained at 514.5 nm laser excitation on a Renishaw Microscope System RM2000 at room temperature. The laser power density was kept less than 3 mW with a resolution of 1.5−2.0 cm^{-1} over the spectral window. Spectra were collected at various locations on each sample studied to determine reproducibility. Wide-angle X-ray diffraction (WAXD) was carried out using a Y-2000 X-ray Diffractometer with CuKα radiation (λ = 0.15406 nm) operating at 40 kV and 40 mA. Differential scanning calorimetry (DSC) was carried out using TA-Q100 at a heating and cooling rate of 10 °C/min under a nitrogen atmosphere. Samples with a typical mass of 5 mg were encapsulated in sealed aluminum pans. All the samples used for FTIR, Raman, WAXD, and DSC characterization were prepared by drying the solutions in a vacuum oven at 35 °C.

Results and Discussions

Morphologies of PE and PEO on the Surface of SWNTs. Figure 1 show TEM images of PE/SWNT and PEO/SWNT nanohybrids prepared in SC CO_2 condition. The periodic patterning of PE on SWNTs to form NHSK structure is shown in Figure 1a,b, where CNTs serve as the shish and PE crystals are the kebabs, which is similar to the classic "shish-kebab" polymer crystals formed in an elongation/shear flow field.[47] As marked by the arrows in Figure 1b, the shish consists of small SWNT bundles, and the surfaces of SWNT bundles are wrapped by a homogeneous polymer coating between each two adjacent kebabs instead of the naked SWNTs. The TEM images of the patterning behavior of PEO show that the whole individual or small bundles of SWNTs are only wrapped by a thin amorphous polymer coating (Figure 1c,d). These distinct results of the high-crystalline polymers wrapping on SWNTs motivate us to investigate the main reason of the formation of various patterns on CNTs.

Effect of the Molecular Structural Factors on the Morphology of Polymers on SWNTs. Recently, many researchers utilized polymer-controlled crystallization method to successfully obtain periodic ordered crystals on CNTs. Up to now, the ordered nanohybrid structures such as transcrystallization and shish-kebab crystals of crystalline polymers on CNTs have been reported in the case of polypropylene (PP), nylon-6, PE, nylon-66, poly(butylenes terephthalate) (PBT), and PVA, indicating that CNTs not only nucleate polymer crystallization, but also act as a template for polymer orientation.[29−37,48,49] Through comparing these reported results referred above, we find an interesting rule that the chain conformation in the unit-cell of polymers such as polyamide, PVA, PE, and polyester are all planar zigzag or zigzag conformations except for PP. As for PP and PEO with helical conformation in crystal, the identity period of PP is far less than that of PEO (the identity period of PP is 0.65 nm, and for PEO is 1.93 nm).[50] Lotz et al. also pointed out that although the crystalline structures of PE and isotactic polypropylene (iPP) are different (PE chain is in planar zigzagged conformation and the unit cell belongs to orthorhombic system, and iPP prefers to form a 3/1 helix conformation and monoclinic system in unit cell), the space between methyl rows in the direction of the axis of *a*, *c* of iPP is similar to that of molecular chains within the axis of *b*, *c* of PE. Therefore there are many substrates that not only can induce PE but also can induce iPP epitaxy growth.[51] Liu et al. also reported that PP adopts a zigzagged conformation on the nanotubes surface instead of helical conformation.[19]

The conformations of PE and PEO in crystal are shown in Figure 2, where PE is planar zigzagged conformation and PEO is helical conformation in the unit-cell. The 7/2 helical conformation in a unit cell makes the chain diameter of PEO much larger than that of PE, which may hinder a close contact with CNTs. As mentioned before, PE chains are random coils in solution,[52] while the PEO molecule is supposed to have both coils and helices in solution.[53] Therefore, the PE coils can translate into a zigzag conformation in the process of crystal growth and then fold into lamellae perpendicular to the CNTs.

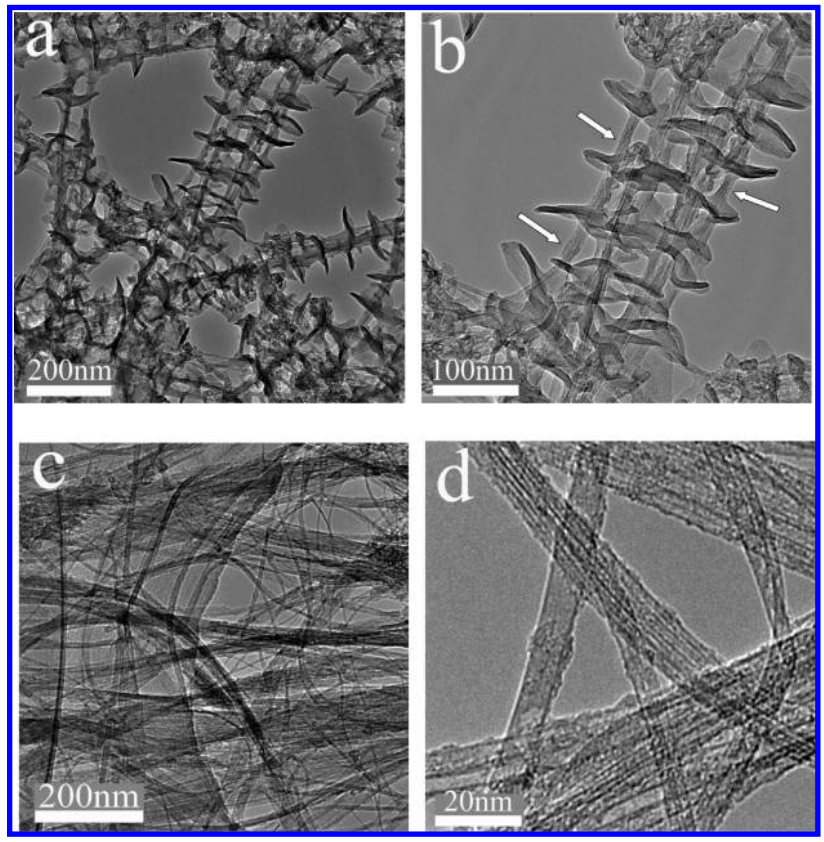

Figure 1. Transmission electron micrographs of nanohybrids prepared in SC CO_2 using two different polymers: (a,b) TEM images of PE-decorated SWNTs, nanohybrid "shish-kebab" structure was formed in SC CO_2 condition at 110 °C and 9.0 MPa for 3 h, and PE concentration and SWNT concentrations are 0.01 and 0.002 wt % in *p*-xylene, respectively; (c,d) TEM images of PEO-decorated SWNTs, produced in SC CO_2 condition of 50 °C and 13.0 MPa for 3 h, and PEO concentration and SWNT concentrations are 0.01 and 0.002 wt % in DMF, respectively.

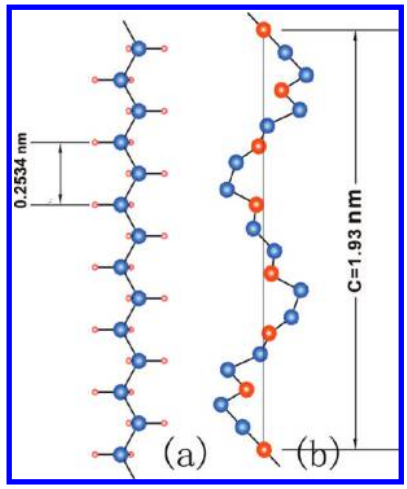

Figure 2. (a) Planar zigzag chain conformation of PE; (b) helical chain conformation of PEO.[50]

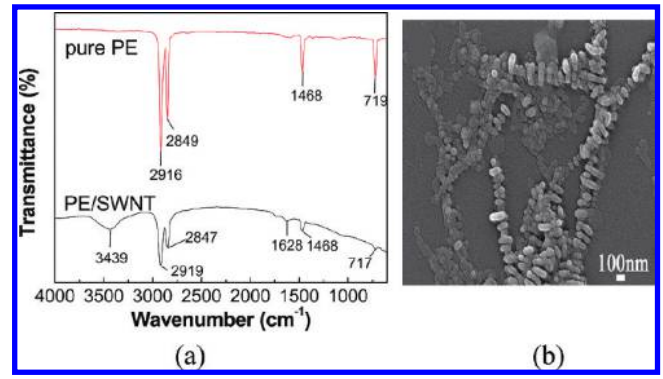

Figure 3. (a) FT-IR spectra of pure PE and PE/SWNT nanohybrid; (b) SEM image of the PE/SWNT nanohybrid. The PE/SWNT nanohybrid was produced in SC CO_2 condition at 100 °C and 16.0 MPa for 3 h, and PE concentration and SWNTs concentrations are both 0.006 wt % in DCB.

The PEO chains prefer to form a 7/2 helix conformation in a unit cell, and epitaxy of helical polymer should be less favorable than the planar zigzag polymer on purely geometrical ground of CNTs; the lower symmetry of the helix and its usually large diameter reduce the regularity and density of polymer−substrate contacts.

Effect of the Interactions between Molecular Chains and SWNTs on the Morphology of Polymers on SWNTs. FT-IR spectroscopy and Raman spectroscopy were used to investigate the interfacial interaction between the polymer molecules and SWNTs. The FTIR spectra for pure PE and PE/SWNT nanohybrid are shown in Figure 3a. The corresponding electron micrographs of PE/SWNT nanohybrid are placed in Figure 3b. Obviously, the characteristic spectra of PE are also present in the PE/SWNT nanohybrid. The two split peaks near 2915 and 2850 cm^{-1} are assigned to the asymmetric and symmetric $-CH_2$ stretching vibration; the doublets at about 1470 and 720 cm^{-1} fall within the range of the $-CH_2$ bending and rocking vibrations, respectively.[54] Nevertheless, the PE/SWNT nanohybrid shows minute broadening and shift in certain regions of the spectrum (Figure 3a). The spectrum was recorded with a resolution of 2 cm^{-1} and hence the shift ≥ 2 cm^{-1} should be considered. The changes in the vibration frequencies of the nanohybrid against the pure polymer are shown in Table 1. Baskaran et al. reported that the presence of interactions of CH groups of polymer with CNTs would shift the frequency of the

TABLE 1: Frequency Shifts of CH Stretching (CH_s) and Bending (CH_b) Vibrations ($\Delta\nu$) in PE and PE/SWNT Nanohybrid

samples	ν or $\Delta\nu$ CH_s, cm^{-1}	ν or $\Delta\nu$ CH_b, cm^{-1}
PE	2916/2849	1468/719
PE/SWNT	$+3/-2^a$	$0/-2^a$

[a] Changes in the vibration frequencies of the nanohybrid against the pure polymer.

CH stretching and bending vibrations of the polymer, and the noncovalent and nonspecific CH$-\pi$ interactions between polymers and carbon nanotubes could lead polymers to coat or wrap on the CNTs.[55] In addition, the intensity of the CH frequencies in the nanohybrid is attenuated noticeably, which further indicates that there exist physical interactions between PE molecules and SWNTs. It is highlighted that the peaks at around 3439 and 1628 cm^{-1} presented in the nanohybrid are assigned to C═O and −OH stretching vibration on the surface of SWNTs due to the purification.[56] There is no other new band in the nanohybrid, which also proves that PE-modified SWNTs belongs to a noncovalent method. The SEM image in Figure 3b shows that the SWNTs are decorated densely by the disk-shaped PE crystals, and some PE lamellae even merge together as a duo to the dense nucleus on the SWNTs. The favorable physical interaction between SWNT bundles and PE chains may lead to a remarkable nucleation effect and thus the PE chains can easily adsorb onto the SWNT surface and crystallize.

Figure 4 shows the FTIR spectra from 4000 to 400 cm^{-1} for pure PEO and PEO/SWNT nanohybrid. Table 2 summarizes the frequencies of all the important absorption bands and the associated assignments. The most significant changes have been marked in Figure 4A. Pure PEO shows a large broad band of asymmetric $-CH_2$ stretching between 3000 and 2750 cm^{-1} with two narrow bands of lower intensity at 2741 and 2696 cm^{-1}. In the nanohybrid, these bands are transformed in two well-defined bands at 2924 and 2858 cm^{-1}, whereas the narrow peaks disappear, which have been reported previously.[57,58] Note that the bands at 2241, 2165, and 1967 cm^{-1}, indicated by upward arrows in the spectrum of pure PEO sample (Figure 4A), are not observed for the nanohybrid.[58] In the region of 1200−1000 cm^{-1} as shown in Figure 4B, it is highlighted that the peak near 1098 cm^{-1} in PEO is for asymmetric stretching vibration of the C−O groups.[58] Whereas, the C−O stretching vibration of the nanohybrid has shifted toward higher frequency of 1103 cm^{-1} compared to that of pure PEO. Analysis of the spectra of PEO and PEO/SWNT nanohybrid indicates that SWNTs show significant influence on the C−O and C−H stretching vibrations of PEO. It could be evidence for presence of interactions between the PEO chains and SWNTs.

Aranda and Ruiz-Hitzky[59,60] claimed that the presence of two bands near 945 and 850 cm^{-1} were assigned to the CH_2 rocking vibrations of methylene groups in the gauche conformation, as required for a helical PEO conformation. The absence of a characteristic IR band near 1320 cm^{-1} assigned to CH_2 stretching vibration of ethylene groups in the trans conformation also confirms the helical structure of PEO.[61] To highlight this observation, detailed spectra between 1800 and 800 cm^{-1} in Figure 4A are enlarged and shown in Figure 4C. In this study, the two bands at 960 and 842 cm^{-1}, which have been related to helical structure, are clearly observed in both the pure PEO sample and the nanohybrid, but the bands in the hybrid become weaker. The characteristic band near 1320 cm^{-1} for CH_2 trans-conformation (illustrated by short black lines) is absent in both samples as shown in Figure 4C. The two bands of CH_2 twisting

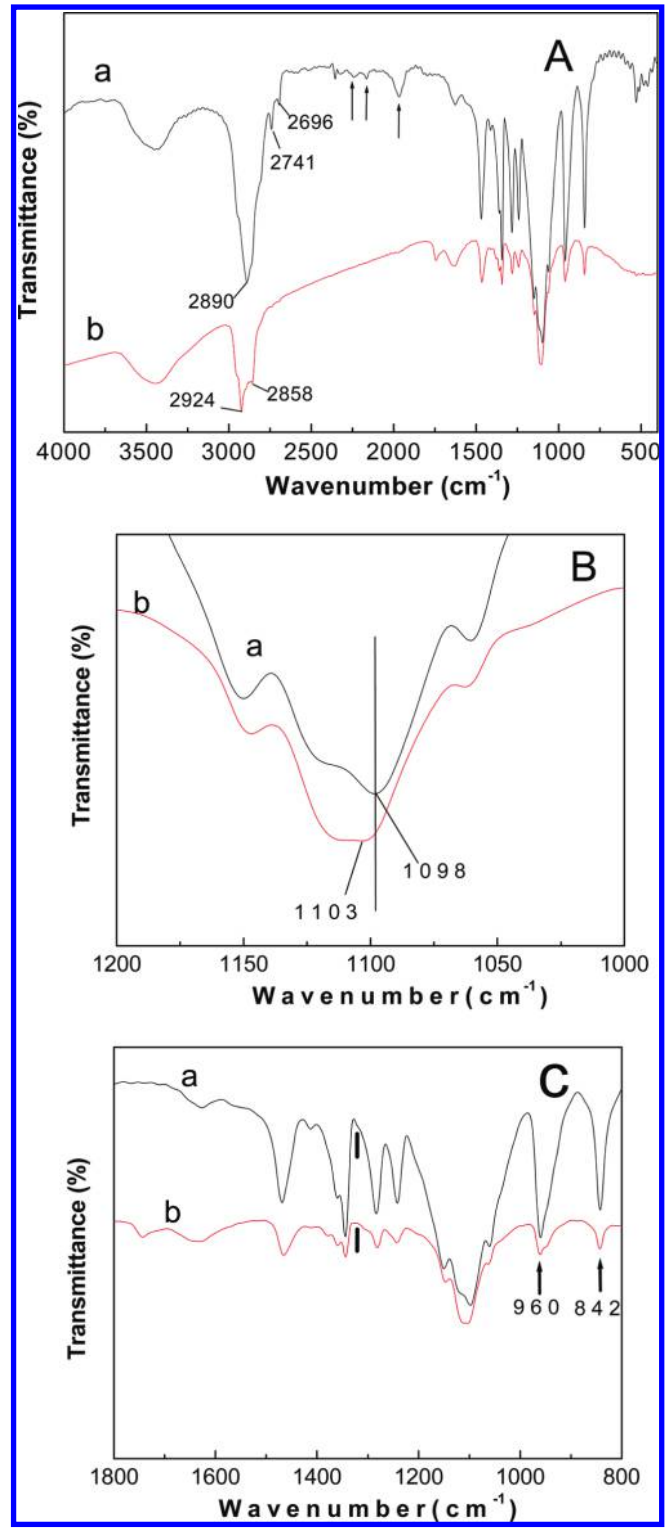

Figure 4. FTIR spectra (A) from 4000 to 400 cm^{-1}, (B) from 1200 to 1000 cm^{-1} and (C) from 1800 to 800 cm^{-1}, for (a) pure PEO and (b) PEO/SWNT nanohybrid produced in SC CO_2 condition at 50 °C, 13.0 MPa for 3 h, and PEO concentration and SWNTs concentrations are 0.01 wt % and 0.002 wt % in DMF, respectively.

vibration at 1283 and 1242 cm^{-1} in pure PEO also become weaker in the nanohybrids, like in PEO-clay complexes.[58] Since the IR absorption bands of the nanohybrid are compared to that of crystalline PEO with a helical conformation, it indicates that in the nanohybrid the helical structure of PEO is more or less distorted, or stretched, but still exists. On the basis of the results

TABLE 2: FTIR Absorption Bands and Their Assignments of PEO and PEO/SWNT Nanohybrid (4000−400 cm^{-1})[a]

frequency (cm $^{-1}$)	frequency in reference (cm $^{-1}$)	assignment	material	reference
3000−2750	3000−2750,[43,57] 2940−2840[58]	$\nu(CH_2)_a$	PEO	43, 57, 58
2924	2925−2875[43]	$\nu(CH_2)_a$	Hybrid	43
2890	2887[62]	$\nu(CH_2)_s$	PEO	62
2858	2925−2875[43]	$\nu(CH_2)_a$	Hybrid	43
2741	2739,[57] 2741[63]	$\nu(CH_2)$	PEO	57, 63
2696	2693,[57] 2696[63]	$\nu(CH_2)$	PEO	57, 63
2241	2240[58,63]		PEO	58, 63
2165	2170,[58] 2172[63]		PEO	58, 63
1967	1970,[58] 1968[63]		PEO	58, 63
1360	1358,[57] 1356,[58] 1360[59]	$\delta(CH_2)_a$	PEO, hybrid	57−59
1344	1342[57,59]	$\delta(CH_2)_a$	PEO, hybrid	57, 59
1283	1282,[58] 1283[61]	$t(CH_2)_a$	PEO, hybrid	58, 61
1242	1242,[58] 1244[61]	$t(CH_2)_a$	PEO, hybrid	58, 61
1098	1109,[43] 1116,[57] 1100,[58] 1103[61]	$\nu(COC)_a$	PEO	43, 57, 58, 61
1103	1116[43]	$\nu(COC)_a$	hybrid	43
960	962[57,58]	$r(CH_2)_a$	PEO, hybrid	57, 58
842	842,[57] 840[58]	$r(CH_2)_s$	PEO, hybrid	57, 58

[a] Mode assignments: ν (stretching); δ (bending); t (twisting); r (rocking). The subscripts a and s denote the asymmetric and symmetric motions with respect to the twofold axis perpendicular to the helix axis and passing through the O atom or through the center of the C−C bond.

of FT-IR studies, the presence of a distorted helical structure of PEO in the nanohybrid is confirmed.

Further evidence for interconnectivity of SWNTs with a polymer was obtained from Raman spectroscopy of the nanohybrids. Figure 5 shows the high frequency Raman spectra for SWNTs, PE/SWNT, and PEO/SWNT nanohybrids. In this part of the spectra, SWNTs display two characteristic peaks, a strong peak (G band), which represents the high-frequency E_{2g} Raman scattering mode of sp^2-hybridized carbon material, and a weak peak assigned to the D band, which may be derived from disordered graphite structures.[37] In Figure 5A, we observe that the intensity of the D band in the spectra of the PEO/SWNT and PE/SWNT nanohybrids has not changed with respect to the SWNTs, unlike the case of functionalized SWNT, where a clear shift was reported.[64] In addition, the degree of graphitization is an indicator of the carbon nanotubes' disorder level and is characterized by the intensity ratio of the D and G bands ($R = I_D/I_G$). The intensity ratios obtained from Figure 5A are 0.22, 0.24, and 0.10 for PEO/SWNT, PE/SWNT, and SWNT, respectively. These similar low values indicate that the electronic structure of the SWNTs is preserved perfectly by the noncovalent wrapping of polymers.

The Raman spectra of the tangential mode of pure SWNTs, PE/SWNT, and PEO/SWNT nanohybrids are shown in Figure 5B. In the tangential mode region, each peak is shifted to higher frequency in the polymer/SWNT nanohybrids compared to the pure SWNTs (2 cm^{-1} for PE/SWNT nanohybrid, and 5 cm^{-1} for PEO/SWNT nanohybrid). Similar up-shifting of the G band has been reported for SWNT-reinforced epoxy resins[65] and polypropylene.[66] Hadjiev et al.[65,67] and Qin et al.[68] reported that the graphite-like G modes of Raman spectra exhibit a upward shift when the nanotubes disperse well in the polymer matrix. As shown in Figure 1, the dispersity of SWNTs in PE/SWNT nanohybrid is much better than that of PEO/SWNT nanohybrid for the PE kebab crystals can serve as spacers to prevent SWNTs from aggregation. Whereas, the higher upshift of the G band for PEO/SWNT nanohybrid further indicates that the interactions between polymers and SWNTs may be another important factor to affect the shift in G-band. Baskaran et al.[55] and McNally et al.[69] pointed out that the up-shifting of the G bands is a consequence of interactions associated with polymer chains with CNTs. Xu et al.[70] used solid-state ^{13}C NMR and Raman to study the packing structure of PEO/MWNT. They demonstrated that there exist n−π-interactions between the n-orbitals of PEO ether oxygen and the π-system of MWNT, which led to the amorphous PEO chains grafted on the MWNT and an upshift in the G-band of the Raman spectra compared to that of neat MWNT. Because of this, special n−π interactions restrict ordered alignment of PEO chains on the surface of CNTs, thus limiting the crystallization of PEO.

From the above discussion, we can conclude that the molecular conformation and the interactions between polymer chains and CNTs indeed play decisive roles on the morphology of microscopic nanohybrid structure. The zigzag conformation of PE chains and the favorable physical interaction between SWNT bundles and PE chains may lead to a remarkable nucleation effect, and thus the PE chains can easily adsorb onto the SWNT surface and crystallize to form the unique NHSK architecture. The distorted helical conformation and special unfavorable interaction with CNTs may prevent PEO from forming periodic ordered crystals on CNTs. In the following, we will discuss the effect of SWNTs on the crystallization behavior of PE and PEO.

Role of SWNTs on Shaping the Semicrystalline framework of PE and PEO. To obtain an understanding of the role of SWNTs on shaping the semicrystalline framework of PE and PEO, WAXD and DSC experiments were carried out. The WAXD patterns of pure PE, PE/SWNT nanohybrid, pure PEO, and PEO/SWNT nanohybrid are displayed in Figure 6. As shown in PE and PE/SWNT nanohybrid patterns, they exhibit two distinct peaks at 2Ω of 21.6 and 24°, corresponding to the (110) and (200) reflections from the orthorhombic unit cell of PE.[27] In PEO and PEO/SWNT nanohybrid patterns, there are two strong peaks occurring at 2Ω = 19.2 and 23.3°, associated with (120) and (112)/(004) reflections from the PEO crystallites.[71] Since the position of the Bragg diffraction peaks of PE/SWNT or PEO/SWNT do not shift significantly with respect to those of neat polymer, the incorporation of SWNTs produces no apparent change in unit cell dimensions and hence in crystal structure. In addition, the XRD pattern of PEO/SWNT nanohybrid exhibits a broad (002) Bragg reflection at about 2Ω = 26°, which is derived from the ordered arrangement of the

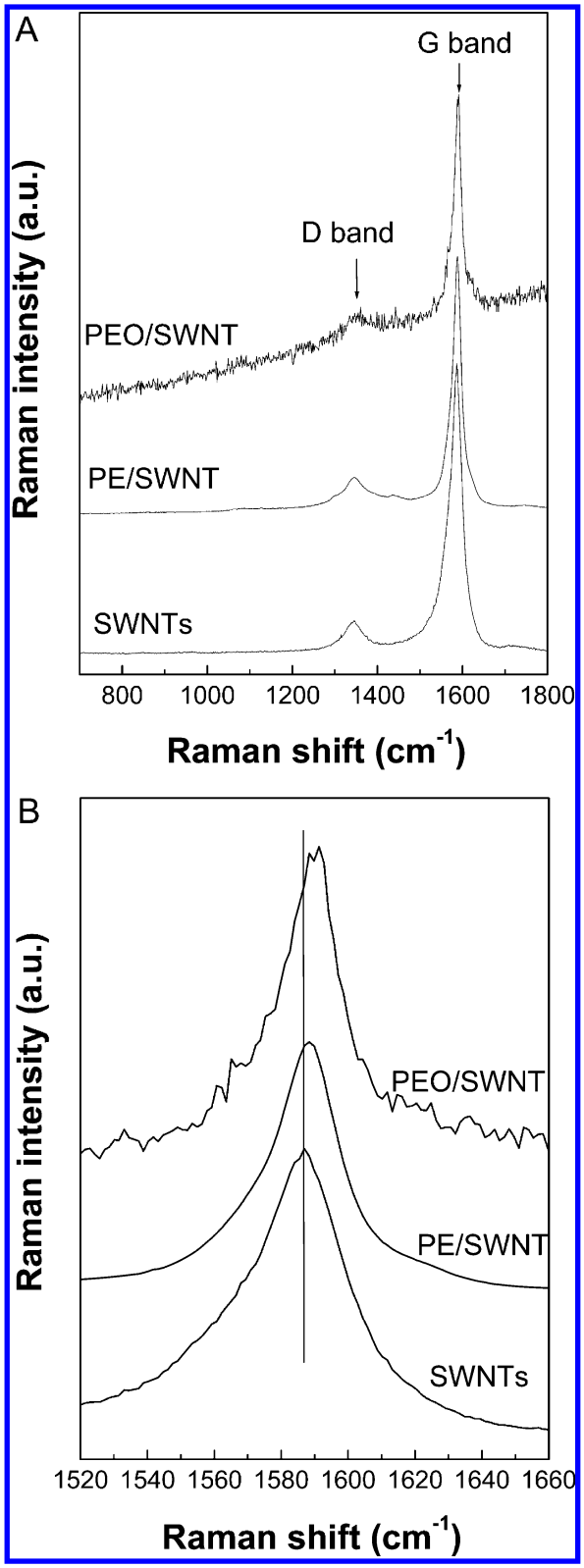

Figure 5. Raman spectra highlight (A) the D and G bands and (B) the tangential modes (G-modes) of SWNTs, PE/SWNT nanohybrid, and PEO/SWNT nanohybrid. The PE/SWNT nanohybrid was produced at 100 °C and 16.0 MPa for 3 h, and PE concentration and SWNTs concentrations are both 0.006 wt % in DCB. The PEO/SWNT nanohybrid was produced in SC CO_2 condition at 50 °C, 13.0 MPa for 3 h, and PEO concentration and SWNTs concentrations are 0.01 and 0.002 wt % in DMF, respectively.

concentric cylinders of graphitic carbon.[72] However, no apparent signal of (002) reflection is observed in the XRD patterns of

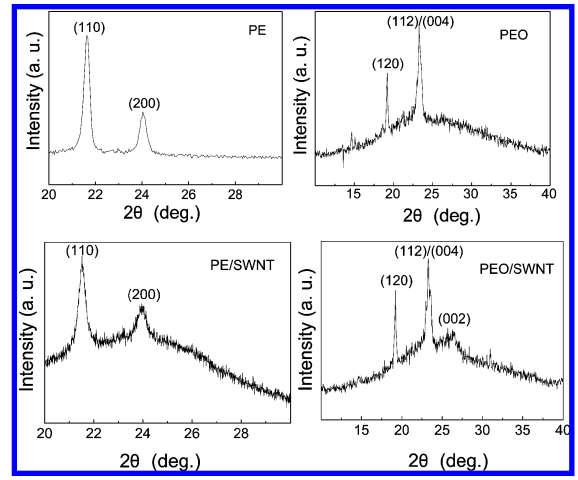

Figure 6. Wide-angle X-ray diffraction patterns of crystals of pure PE, PE/SWNT nanohybrid, pure PEO, and PEO/SWNT nanohybrid. The PE/SWNT nanohybrid was produced at 100 °C and 16.0 MPa for 3 h, and PE concentration and SWNTs concentrations are both 0.006 wt % in DCB. The PEO/SWNT nanohybrid was produced in SC CO_2 condition at 50 °C, 13.0 MPa for 3 h, and PEO concentration and SWNTs concentrations are 0.01 and 0.002 wt % in DMF, respectively. The pure PE and pure PEO were treated in the same SC CO_2 condition as the corresponding nanohybrid.

PE/SWNT nanohybrid, which further proves the efficient dispersion of SWNTs by the special confinement of PE kebab.

To investigate the effect of SWNTs on the crystallization behavior of PE and PEO after SC CO_2 treatment, the first heating DSC trace was used for analysis without regard to the thermal history. The corresponding DSC thermograms of pure PE, PE/SWNT nanohybrid, pure PEO, and PEO/SWNT nanohybrid heated at 10 °C/min rate are shown in Figure 7. The melting temperature, Tm, and degree of crystallinity, X_c, are listed in Table 3. As shown in Figure 7A, the melting temperature, Tm, obtained from the endothermic peak is about 127.9 °C for pure PE. The addition of SWNTs into PE leads to a slight shift toward lower Tm, 126.4 °C. The crystallinity of PE in the nanohybrid depresses compared to the pure PE. The NHSK structure shows that SWNTs serve as a good heterogeneous nucleating agent for PE. This contradiction can be explained as the following: SWNTs provide heterogeneous nucleation sites for PE crystallization while the NHSK structure hinders polymer chain diffusion and crystal growth, which led to lower Tm and X_c for the nanohybrid. DSC heating curves of pure PEO and PEO/SWNT nanohybrid are shown in Figure 7B. It is clearly observed that the introduction of SWNTs results in a dramatic decrease in the melting temperature and crystallinity of the PEO/SWNT nanohybrid, though the SWNTs content of PEO/SWNT nanohybrid is much lower than that of PE/SWNT nanohybrid. It suggests that the incorporation of SWNTs can significantly disrupt the crystallization process of PEO in SC CO_2 due to the antinucleation effect of SWNTs on PEO.

Mechanism Analysis of the Formation of Different Morphologies on SWNTs. According to the formation mechanism of the unique NHSK structure, the most popular explanation is that "epitaxy" and "geometry confinement" are two main factors to affect the NHSK structure, in which polymer chains directly nucleate on the sidewall of CNTs.[37] Nevertheless, as indicated from the TEM image (Figure 1b), the surfaces of small SWNT bundles are wrapped by a homogeneous polymer coating between each two adjacent kebabs. Zhang et al. recently also proposed that a homogeneous polymer coating played a key role in the formation of NHSK structures.[75]

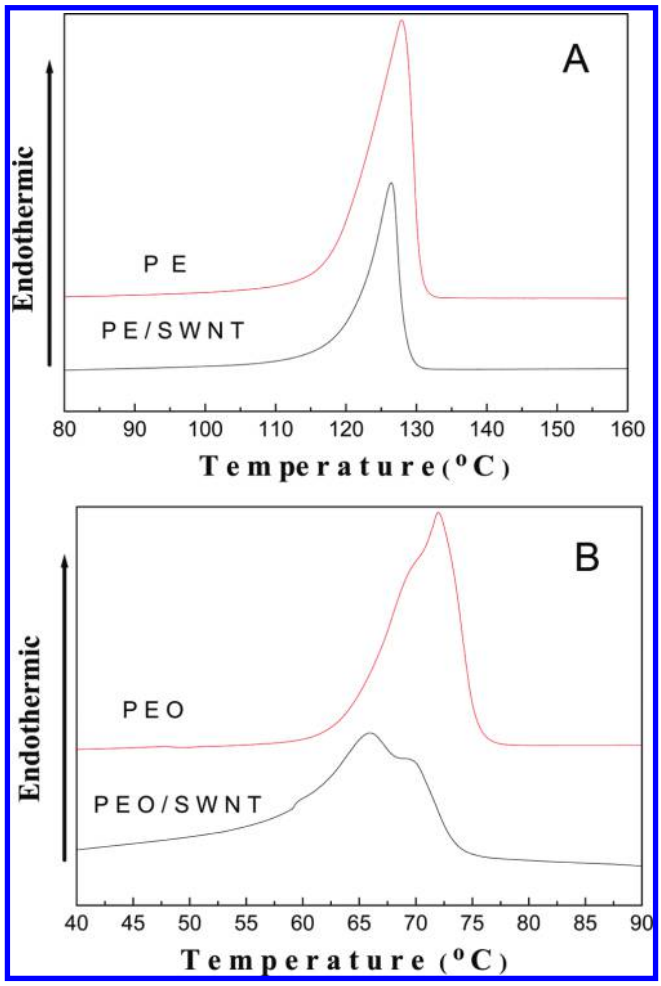

Figure 7. Nonisothermal DSC scans of (A) pure PE and PE/SWNT nanohybrid, (B) pure PEO and PEO/SWNT nanohybrid. The PE/SWNT nanohybrid was produced at 100 °C and 16.0 MPa for 3 h, and PE concentration and SWNTs concentrations are both 0.006 wt % in DCB. The PEO/SWNT nanohybrid was produced in SC CO_2 condition at 50 °C, 13.0 MPa for 3 h, and PEO concentration and SWNTs concentrations are 0.01 and 0.002 wt % in DMF, respectively. The pure PE and pure PEO were treated in the same SC CO_2 condition as the corresponding nanohybrid.

TABLE 3: Melting Temperatures (Tm, °C), Heats of Fusion (ΔH_i, J/g), and Weight Fractional Crystallinities (X_c, %) of Pure PE, PE/SWNT Nanohybrid, pure PEO, and PEO/SWNT Nanohybrid

samples	Tm	ΔH_i (J/g)	X_c (%) [b]
PE	127.9	174.3	59.5
PE/SWNT (50 wt % SWNTs)[a]	126.4	77.8	53.1
PEO	72.0	128.6	62.7
PEO/SWNT (16.7 wt % SWNT)[a]	66.0	43.3	25.4

[a] The contents of SWNTs were calculated from the PE/SWNT and PEO/SWNT solutions prepared in SC CO_2. [b] The weight fractional crystallinities of the samples were calculated by the equation: X_c (%) = $\Delta H_i/f_i\Delta H_i^m \times 100\%$, where ΔH_i is the enthalpy of fusion of the prepared samples, directly obtained by DSC, and f_i is the mass fraction of polymer in the hybrids. ΔH_i^m, the enthalpy of fusion of 100% crystalline polymer, are 293 J/g for PE[73] and 205 J/g for PEO.[74]

The controversial explanation is owing to the different understandings of the early stage nucleation modes. Kaito et al. indicated that nucleation in epitaxial growth may be described as either two-dimensional (2D) mode or three-dimensional (3D) mode, depending on whether the substrate is covered with a monolayer of epitaxially grown crystals before proceeding to homogeneous crystal-growth or if 3D epitaxial nuclei have formed directly on the substrate. A high adhesion energy between the two phases is critical for 2D epitaxial growth.[76] The bonding strength between the SWNTs and the polymers can be evaluated by interfacial energy in the composites.[77] The total interaction energy, $E_{interaction}$, is twice the interfacial binding energy γ scaled by A, where A is the contact area between polymer and SWNT surface[78]

$$E_{interaction} = 2\gamma A$$

Some molecular dynamics (MD) simulation studies showed that the PE chains preferred the extended conformation or ordered orientation structure along the tube axis in the first adsorption layer due to the strong van der Waals interaction between PE chains and CNTs.[18,19] The extended conformation or ordered orientation structure can result in a larger A, and therewith obtain high adhesion energy between PE chains and CNTs. Therefore, we conclude that the early stage nucleation mode of PE on CNTs should adopt a 2D mode, which PE prefers to form a homogeneous coating along the tube axis before proceeding to kebab crystal growth. To further confirm the growth process of periodical PE crystal lamellae, a series of TEM images of the intermediate state of PE lamellae-modified MWNTs process are shown in Figure 8. It is obvious that there are only some molecular chains deposited on the MWNTs surface at the initial state. In Figure 8b, it seems that the PE chains form a thin layer around MWNTs. As shown in Figure 8c, the PE layer becomes thicker, and subglobules (shown by white arrow) are formed on the homogeneous layer, which may serve as nuclei for the growth of crystal lamellae. The periodical PE crystal lamellae are finally formed in Figure 8d.

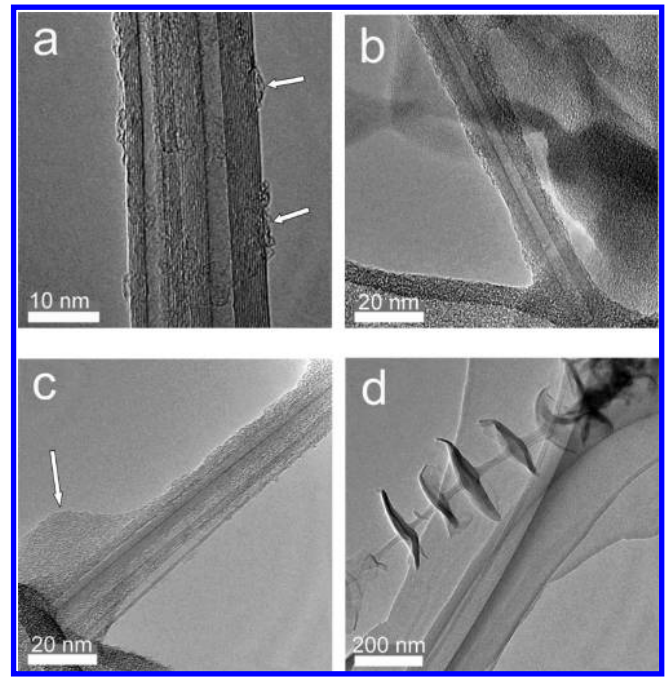

Figure 8. Groups of TEM images of PE/MWNT NHSK structure formed in PE concentration (0.006 wt %) and MWNTs concentration (0.002 wt %) in *p*-xylene, and at SC CO_2 condition of 100 °C/9 MPa for 3 h. (a) Some molecular chains deposit on the MWNTs surface; (b) a thin layer PE molecules patterning around MWNTs; (c) subglobules (shown by white arrow) are formed on the homogeneous layer; (d) formation of crystal lamella.

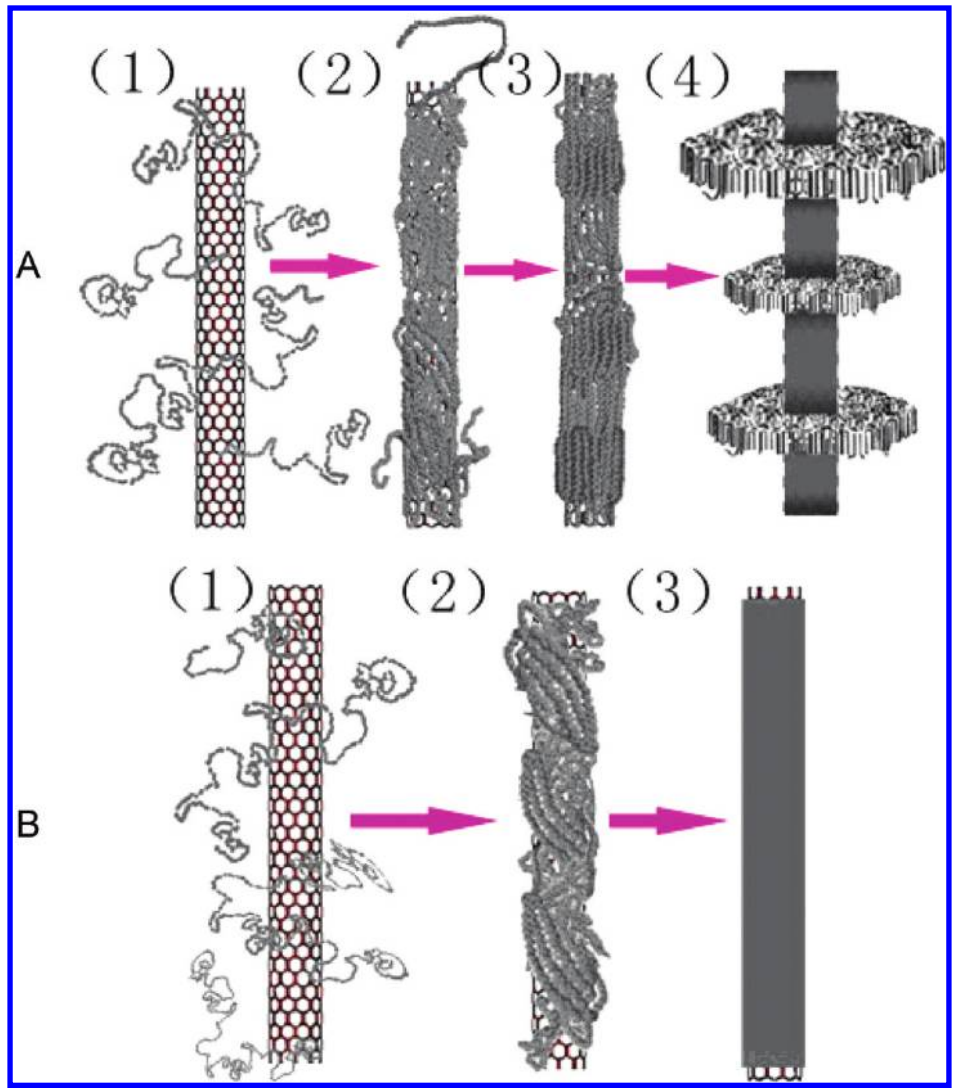

Figure 9. Schematic representations of the hypothetical mechanism of (A) PE/SWNT and (B) PEO/SWNT nanohybrid superstructures formation process.

On the basis of the above results, we prefer to present schematic representation of the hypothetical formation mechanism of PE and PEO on SWNTs, as shown in Figure 9 and interpreted in detail as following. In an initial situation, random-coil PE chains exist in the solution of PE/SWNT system (Figure 9A-1). First, some segments of PE chains near the SWNTs are adsorbed onto the SWNT surfaces by the attractive van der Waals interactions. The adsorbed chains wrap along the SWNT surfaces and drag their neighboring chains onto the SWNT surfaces. Second, the adsorbed chains begin to slide along the tubes into a homogeneous layerlike local-ordered structure (Figure 9A-2). Subsequently, in Figure 9A-3, during the polymer chain relaxation and orientation, a subglobule will appear on the ordered structure, which is considered as the crystal nucleus. Finally, with the increasing amount of PE wrapping, PE chains begin to epitaxially grow from the subglobules with folded-chain shape to decrease the polymer surface energy and grow perpendicular to the SWNTs long axis, obeying the "soft epitaxy" crystallization mechanism. In the end, a typical NHSK structure is formed, as shown in Figure 9A-4.

A general thermodynamic driving force for multihelical wrapping associated with linear polymer around SWNTs in an aqueous environment has been identified by O'Connell et al. The helical wrapping allows high-surface area coverage with low-backbone strain.[5] The noncovalent and nonspecific CH$-\pi$ interactions between polymers and carbon nanotubes could lead polymers to coat or wrap on the CNTs.[55] For PEO, its intrinsic helical conformation and the unfavorable interactions with CNTs causes a distorted helix structure around the nanotube (Figure 9B-2). Finally, with the increasing amount of PEO wrapping, the whole surface of SWNTs are wrapped with a thin homogeneous coating in amorphous phase, as shown in Figure 9B-3.

Conclusions

In this article, we reported a comparison study of morphology and crystallization behavior of PE and PEO on SWNTs with assistance of SC CO_2. PE/SWNT nanohybrid shish-kebab structure was achieved using SC CO_2 SAIPE method. For PEO modification on SWNTs, a homogeneous coating was obtained.

On the basis of the analysis of molecular structural factors and the results from FT-IR and Raman spectra, it revealed that the morphology of the nanohybrids was found to depend on the molecular conformation and the interactions between polymer chains and SWNTs. The zigzag conformation of PE chains and their favorable physical interactions with SWNTs led to a remarkable nucleation effect, and thus the PE chains can easily adsorb onto the SWNT surface and crystallize to form the unique NHSK architecture. The distorted helical conforma-

tion and special unfavorable interaction with SWNTs prevented PEO from forming periodic ordered crystals on SWNTs. The effects of SWNTs on the crystallization behaviors of PE and PEO were examined by WAXD and nonisothermal experiments. The WAXD results suggested that the incorporation of SWNTs produced no apparent change in crystal structure of the two polymers. The slight reduction of melting temperature and crystallinity of PE/SWNT nanohybrid showed that SWNTs provided heterogeneous nucleation sites for PE crystallization while the NHSK structure hindered polymer chain diffusion and crystal growth. The dramatic decrease in the melting temperature and crystallinity of the PEO/SWNT nanohybrid suggested that SWNTs played an antinucleation effect on PEO. Also, the formation mechanism analysis indicated that PE chains preferred to form a homogeneous coating along the tube axis before proceeding to kebab crystal growth.

This work is a preliminary stage for a series of systematic profound investigations concerned preparation of more precisely hierarchical structures on CNTs in a facile way, which is a key step toward using one-dimensional nano- materials in nanodevice applications.

Acknowledgment. We are grateful for the National Natural Science Foundation of China (No. 20974102, 50955010), the financial support from the Program for New Century Excellent Talents in Universities (NCET) and from the Ministry of Personnel of China.

References and Notes

(1) Chen, J.; Hamon, M. A.; Hu, H.; Chen, Y. S.; Rao, A. M.; Eklund, P. C.; Haddon, R. C. *Science* **1998**, *282*, 95–98.
(2) Ausman, K. D.; Piner, R.; Lourie, O.; Ruoff, R. S.; Korobov, M. *J. Phys. Chem. B* **2000**, *104*, 8911–8915.
(3) Dai, L.; Mau, A. W. H. *Adv. Mater.* **2001**, *13*, 899–913.
(4) Bekyarova, E.; Itkis, M. E.; Cabrera, N.; Zhao, B.; Yu, A. P.; Gao, J. B.; Haddon, R. C. *J. Am. Chem. Soc.* **2005**, *127*, 5990–5995.
(5) O'Connell, M. J.; Boul, P.; Ericson, L. M.; Huffman, C.; Wang, Y. H.; Haroz, E.; Kuper, C.; Tour, J.; Ausman, K. D.; Smalley, R. E. *Chem. Phys. Lett.* **2001**, *342*, 265–271.
(6) Zhang, J.; Lee, J.-K.; Wu, Y.; Murray, R. W. *Nano Lett.* **2003**, *3*, 403–407.
(7) Matarredona, O.; Rhoads, H.; Li, Z.; Harwell, J. H.; Balzano, L.; Resasco, D. E. *J. Phys. Chem. B* **2003**, *107*, 13357–13367.
(8) Katz, E.; Wilner, I. *Chem. Phys. Chem.* **2004**, *5*, 1084–1104.
(9) Tang, B. Z.; Xu, H. *Macromolecules* **1999**, *32*, 2569–2576.
(10) Biercuk, M. J.; Llaguno, M. C.; Radosavljevic, M.; Hyun, J. K.; Johnson, A. T.; Fischer, J. E. *Appl. Phys. Lett.* **2002**, *80*, 2767–2769.
(11) Liu, T.; Sreekumar, T. V.; Kumar, S.; Hauge, R. H.; Smalley, R. E. *Carbon* **2003**, *41*, 2440–2442.
(12) Azamian, B. R.; Davis, J. J.; Coleman, K. S.; Bagshaw, C. B.; Green, M. L. H. *J. Am. Chem. Soc.* **2002**, *124*, 12664–12665.
(13) Szleifer, I.; Yerushalmi-Rozen, R. *Polymer* **2005**, *46*, 7803–7818.
(14) Nativ-Roth, E.; Shvartzman-Cohen, R.; Bounioux, C.; Florent, M.; Zhang, D.; S- zleifer, I.; Yerushalmi-Rozen, R. *Macromolecules* **2007**, *40*, 3676–3685.
(15) Yang, M. J.; Koutsos, V.; Zaiser, M. *J. Phys. Chem. B* **2005**, *109*, 10009–10014.
(16) Zheng, Q. B.; Xue, Q. Z.; Yan, K. Y.; Hao, L. Z.; Li, Q.; Gao, X. L. *J. Phys. Chem. C* **2007**, *111*, 4628–4635.
(17) Foroutan, M.; Nasrabadi, A. T. *J. Phys. Chem. B* **2010**, *114*, 5320–5326.
(18) Yang, H.; Chen, Y.; Liu, Y.; Cai, W. S. *J. Chem. Phys.* **2007**, *127*, 094902.
(19) Liu, W.; Yang, C. L.; Zhu, Y. T.; Wang, M. S. *J. Phys. Chem. C* **2008**, *112*, 1803–1811.
(20) Wei, C.; Srivastava, D.; Cho, K. *Nano Lett.* **2004**, *4*, 1949–1952.
(21) Wei, C. *Appl. Phys. Lett.* **2006**, *88*, 093108.
(22) Cadek, M.; Coleman, J. N.; Barron, V.; Hedicke, K.; Blau, W. J. *Appl. Phys. Lett.* **2002**, *81*, 5123–5125.
(23) Zhang, F.; Xu, Q.; Zhang, H.; Zhang, Z. W. *J. Phys. Chem. C* **2009**, *113*, 18531–18535.
(24) Ning, N. Y.; Luo, F.; Wang, K.; Zhang, Q.; Chen, F.; Du, R. N.; An, C. Y.; Pan, B. F.; Fu, Q. *J. Phys. Chem. B* **2008**, *112*, 14140–14148.
(25) Li, H. H.; Zhang, X. Q.; Duan, Y. X.; Wang, D. J.; Li, L.; Yan, S. K. *Polymer* **2004**, *45*, 8059–8065.
(26) Haggenmueller, R.; Fischer, J. E.; Winey, K. I. *Macromolecules* **2006**, *39*, 2964–2971.
(27) Trijillo, M.; Arnal, M. L.; Muller, A. J.; Bredeau, S.; Bonduel, D.; Dubois, Ph.; Hamley, I. W.; Castelletto, V. *Macromolecules* **2008**, *41*, 2087–2095.
(28) Vega, J. F.; Martinez-Salazar, J.; Trijillo, M.; Arnal, M. L.; Muller, A. J.; Bredeau, S.; Dubois, Ph. *Macromolecules* **2009**, *42*, 4719–4727.
(29) Li, C. Y.; Li, L. Y.; Cai, W. W.; Kodjie, S. L.; Tenneti, K. K. *Adv. Mater.* **2005**, *17*, 1198–1202.
(30) Zhang, Q.; Lippits, D. R.; Rastogi, S. *Macromolecules* **2006**, *39*, 658–666.
(31) Uehara, H.; Kato, K.; Kakiage, M.; Yamanobe, T.; Komoto, T. *J. Phys. Chem. C* **2007**, *111*, 18950–18957.
(32) García-Gutiérrez, M. C.; Nogales, A.; Rueda, D. R.; Domingo, C.; García-Ramos, J. V.; Broza, G.; Roslaniec, Z.; Schulte, K.; Ezquerra, T. A. *Compos. Sci. Technol.* **2007**, *67*, 798–805.
(33) Liang, S.; Wang, K.; Chen, D. Q.; Zhang, Q.; Du, R. N.; Fu, Q. *Polymer* **2008**, *49*, 4925–4929.
(34) Yue, J.; Xu, Q.; Zhang, Z. W.; Chen, Z. M. *Macromolecules* **2007**, *40*, 8821–8826.
(35) Zhang, Z. W.; Xu, Q.; Chen, Z. M.; Yue, J. *Macromolecules* **2008**, *41*, 2868–2873.
(36) Zhang, F.; Zhang, H.; Zhang, Z. W.; Chen, Z. M.; Xu, Q. *Macromolecules* **2008**, *41*, 4519–4523.
(37) Li, L. Y.; Li, C. Y.; Ni, C. Y. *J. Am. Chem. Soc.* **2006**, *128*, 1692–1699.
(38) Li, L. Y.; Li, B.; Hood, M. A.; Li, C. Y. *Polymer* **2009**, *50*, 953–965.
(39) Li, Y.; Huang, X. J.; Heo, S. H.; Li, C. C.; Choi, Y. K.; Cai, W. P.; Cho, S. O. *Langmuir* **2007**, *23*, 2169–2174.
(40) Li, Y.; Lee, E. J.; Cai, W. P.; Kim, K. Y.; Cho, S. O. *ACS Nano* **2008**, *2*, 1108–1112.
(41) Li, B.; Li, L. Y.; Wang, B. B.; Li, C. Y. *Nat. Nanotechnol.* **2009**, *4*, 358–362.
(42) Chatterjee, T.; Yurekli, K.; Hadjiev, V. G.; Krishnamoorti, R. *Adv. Funct. Mater.* **2005**, *15*, 1832–1838.
(43) Jin, J.; Song, M.; Pan, F. *Thermochim. Acta* **2007**, *456*, 25–31.
(44) Wang, B. B.; Li, B.; X, J.; Li, C. Y. *Macromolecules* **2008**, *41*, 9516–9521.
(45) Shaffer, M. S. P.; Windle, A. H. *Adv. Mater.* **1999**, *11*, 937–941.
(46) Probst, o.; Moore, E. M.; Resasco, D. E.; Grady, B. P. *Polymer* **2004**, *45*, 4437–4443.
(47) Pennings, A. J.; Kiel, A. M. *Kolloid Z. Z. Polym.* **1965**, *205*, 160–162.
(48) Lu, K. B.; Grossiord, N.; Koning, C. E.; Miltner, H. E.; van Mele, B.; Loos, J. *Macromolecules* **2008**, *41*, 8081–8085.
(49) Brosse, A. C.; Tence'-Girault, S.; Piccione, P. M.; Leibler, L. *Polymer* **2008**, *49*, 4680–4686.
(50) Jenkins, A. D. *Polymer Science -A materials science handbook*; North- Holland Publishing Co.: London, 1972; Vol. 1, Chapter 4.
(51) Lotz, B.; Wittmann, J. C. *J. Polym. Sci., Part B: Polym. Phys.* **1987**, *25*, 1079–1087.
(52) De Gennes, P. G. *J. Chem. Phys.* **1970**, *60*, 5030–5042.
(53) Patricia, C.; Norman, A. I.; Greer, S. C. *J. Phys. Chem. B* **2006**, *110*, 22172–22177.
(54) Bower, D. I.; Maddams, W. F. *The vibrational spectroscopy of polymers*; Cambridge University Press: Cambridge; 1989.
(55) Baskaran, D.; Mays, J. W.; Bratcher, M. S. *Chem. Mater.* **2005**, *17*, 3389–3397.
(56) Shieh, Y. T.; Liu, G. L.; Wu, H. H.; Lee, C. C. *Carbon* **2007**, *45*, 1880–1890.
(57) Ratna, D.; Divekar, S.; Samui, A. B.; Chakraborty, B. C.; Banthia, A. K. *Polymer* **2006**, *47*, 4068–4074.
(58) Shen, Z. Q.; Simon, G. P.; Cheng, Y. B. *Polymer* **2002**, *43*, 4251–4260.
(59) Ruiz-Hitzky, E.; Aranda, P. *Adv. Mater.* **1990**, *2*, 545–547.
(60) Aranda, P.; Ruiz-Hitzky, E. *Chem. Mater.* **1992**, *4*, 1395–1403.
(61) Papke, B. L.; Ratner, M. A.; Shriver, D. F. *J. Phys. Chem. Solids* **1981**, *42*, 493–500.
(62) Webb, S. W.; Stanley, D. A.; Scheiner, B. *An infared examination of ionexchanged montmorillonite treated with polyethlene oxide*; RI 9036; U.S. Bureau of Mines: Avondale, MD, 1986.
(63) Hummel, D. O. *Atlas of polymer plastics analysis: Defined polymers*, 3rd ed; Hanser Publishers & VCH Publishers: New York, 1991; Vol. 1 /Band 1, pp 258−9, 460−3.
(64) Lefrant, S.; Baltog, I.; Baibarac, M. J. *Raman. Spectrosc.* **2005**, *36*, 676–698.
(65) Hadjiev, V. G.; Iliev, M. N.; Arepalli, S.; Nikolaev, P.; Files, B. S. *Appl. Phys. Lett.* **2001**, *78*, 3193–3195.
(66) Valentini, L.; Biagiotti, J.; Kenny, J. M.; Santucci, S. *Compos. Sci. Technol.* **2003**, *63*, 1149–1153.

(67) Hadjiev, V. G.; Mitchell, C. A.; Arepalli, S.; Bahr, J. L.; Tour, J. M.; Krishnamo- orti, R. *J. Chem. Phys.* **2005**, *122*, 124708.

(68) Qin, S. H.; Qin, D. Q.; Ford, W. T.; Herrera, J. E.; Resasco, D. E. *Macromolecules* **2004**, *37*, 9963–9967.

(69) McNally, T.; Potschke, P.; Halley, P.; Murphy, M.; Martin, D.; Bell, S. E. J.; Brennan, G. P.; Bein, D.; Lemoine, P.; Quinn, J. P. *Polymer* **2005**, *46*, 8222–8232.

(70) Xu, M.; Chen, Q. *Chin. J. Magn. Reson.* **2007**, *24*, 469–474.

(71) Huang, X. D.; Goh, S. H. *Macromolecules* **2001**, *34*, 3302–3307.

(72) Wei, B.; Vajtai, R.; Choi, Y. Y.; Ajayan, P. M.; Zhu, H.; Xu, C.; Wu, D. *Nano Lett.* **2002**, *2*, 1105–1107.

(73) Na, B.; Wang, K.; Zhang, Q.; Du, R. N.; Fu, Q. *Polymer* **2005**, *46*, 3190–3198.

(74) Shieh, Y. T.; Liu, G. L.; Hwang, K. C.; Chen, C. C. *Polymer* **2005**, *46*, 10945–10951.

(75) Zhang, L.; Tao, T.; Li, C. Z. *Polymer* **2009**, *50*, 3835–3840.

(76) Wang, J.; Kaito, A.; Yase, K.; Tanigaki, N. *Polymer* **1996**, *37*, 3247–3254.

(77) Zheng, Q. B.; Xia, D.; Xue, Q. Z.; Yan, K. Y.; Gao, X. L.; Li, Q. *Appl. Surf. Sci.* **2009**, *255*, 3534–3543.

(78) Lordi, V.; Yao, N. *J. Mater. Res.* **2000**, *15*, 2770–2779.

JP103932B